



Catalytic oxidation of CO over Pt/TiO₂ with low Pt loading: The effect of H₂O and SO₂



Chenglin Feng ^{a,b}, Xiaolong Liu ^{a,*}, Tingyu Zhu ^{a,c,*}, Yutao Hu ^a, Mengkui Tian ^b

^a CAS Key Laboratory of Green Process and Engineering, Institute of Process Engineering, Innovation Academy for Green Manufacture, Chinese Academy of Sciences, Beijing, 100190, China

^b School of Chemistry and Chemical Engineering, Guizhou University, Guiyang, Guizhou, 550025, China

^c Center for Excellence in Regional Atmospheric Environment, Institute of Urban Environment, Chinese Academy of Sciences, Xiamen, 361021, China

ARTICLE INFO

Keywords:

CO
Catalytic oxidation
Water promotion
Reaction mechanism

ABSTRACT

Anatase TiO₂ loaded with 0.1wt.% Pt catalyst (0.1Pt/TiO₂-A) was prepared via the impregnation method, and its CO catalytic oxidation activity was investigated. Noteworthy, introduction of H₂O into the reaction atmosphere apparently facilitated the catalytic oxidation of CO. Besides, introduction of SO₂ inhibited the catalytic oxidation of CO. In presence of H₂O and SO₂, 0.1Pt/TiO₂-A showed outstanding catalytic stability, and X-ray photoelectron spectroscopy (XPS) and thermogravimetric (TG) characterizations suggested that the amount of sulfate species deposited on the 0.1Pt/TiO₂-A treated at 230 °C did not increase with time extension, which might be an important reason for the high sulfur resistance of 0.1Pt/TiO₂-A. XPS results also demonstrated that the dissociation of H₂O led to considerably increase of hydroxyl groups over the catalyst surface. H₂¹⁸O isotope-labeling experiments unambiguously showed that C¹⁶O¹⁸O was the main product accounting for 88.9%, revealing that the other oxygen atom in the product CO₂ was mostly from H₂O. Consequently, based on previous researches and our experimental results, the mechanism of H₂O promoting CO oxidation on 0.1Pt/TiO₂-A catalyst was proposed.

1. Introduction

CO is harmful to the human body mainly produced by incomplete combustion of fossil fuels [1]. Catalytic oxidation is considered as the most effective CO removal method due to its high efficiency and energy saving [2]. In recent years, it has gained increasing importance in indoor air purification [3–6], diesel vehicle exhaust purification [7,8], preferential oxidation of CO (PROX) in proton exchange membrane fuel cells (PEMFC) [9–12], and actual industrial exhaust CO removal [2,13]. Taking into account the large amount of CO emission in industrial flue gas, for example, the concentration of CO in the sintering flue gas emitted from the sintering process of iron and steel industry is 8000–10000 mg/Nm³. Therefore, it is very meaningful to investigate CO removal for industrial flue gas.

As a consequence, much attention has been devoted to develop the catalysts, including noble metals such as Pt [14–16], Pd [17,18], Au [19, 20], Ag [21,22], Rh [23], Ir [24], Ru [25] and transition metals such as Co [26], Ni [27], Cu [28,29]. Previous studies have shown that noble metal catalysts displayed apparently higher catalytic activity than

transition metal catalysts under the reaction atmosphere (CO, O₂) [30]. However, the industrial flue gas still contains certain concentration of SO₂ and H₂O even if the catalytic unit is placed after desulfurization. Therefore, the tolerance of the catalyst under the coexistence of SO₂ and H₂O is very important.

In recent years, the effects of H₂O for CO oxidation behavior and mechanisms are controversial over noble metal catalysts. Laden et al. [31] investigated that the introduction of 4% water on Au/Fe₂O₃ catalyst significantly inhibited CO oxidation at 25 °C, and CO conversion decreased about 40%. Wang et al. [32,33] found that the oxidation of CO over the Pt/Cr_xFe_{2-x}O₃ catalysts were considerably enhanced in presence 10% H₂O, owing to the promotion of CO desorption and then rapid reaction with the hydroxyl groups dissociated from H₂O to form CO₂. Through the H₂¹⁸O isotope-labeling experiments for CO oxidation on the Pt₁/CeO₂ single atom catalyst, Wang et al. [34] revealed that nearly half of the products CO₂ were labeled ¹⁸O with the oxidation temperature higher than 98 °C, giving direct proof that H₂O participated in the CO oxidation. Additionally, over Au/TiO₂, Au/Al₂O₃, and Au/SiO₂ catalysts, Nakamura and Fujitani et al. [35] believed that H₂O

* Corresponding authors at: CAS Key Laboratory of Green Process and Engineering, Institute of Process Engineering, Innovation Academy for Green Manufacture, Chinese Academy of Sciences, Beijing, 100190, China.

E-mail addresses: liuxl@ipe.ac.cn (X. Liu), tuyzhu@ipe.ac.cn (T. Zhu).

could facilitate the stable carbonates into easily decomposable bicarbonates, thereby promoting CO oxidation to CO₂. Besides, Saavedra et al. [36] believed that on the Au/TiO₂ catalyst, water can provide protons to O₂ to form Au-OOH species, which could reduce the energy of the O—O bond breakage to promote the activation of O₂. Au-OOH species react with CO adsorbed on Au sites to form Au-COOH species, and then Au-COOH species decompose to produce CO₂. Hence, it is of great significance to clarify the influence mechanism of H₂O on the catalyst under actual flue gas conditions.

Besides, the ability of SO₂ tolerance for noble metal catalysts strongly depends on the type of active species. For Au-based catalysts, the sulfate formed at the metal-interface inhibited the formation of intermediate carbonates below 200 °C, thereby inhibiting the CO oxidation activity [37–39]. For Pd-based catalysts, the active center could be sulfated into PdSO₄ species and H₂O would accelerate the process of sulfation of Pd species, resulting the catalysts loses CO oxidation activity [40,41]. For Pt-based catalysts, Pt species as the active centers could not be sulfated under oxygen-containing condition, owing to that SO₂ was oxidized to SO₃ at the Pt sites and then quickly migrated to the carriers [42]. However, considering the relatively high cost of Pt, the loading of Pt should be reduced. It was also found that the catalyst with low Pt loading gave high CO catalytic activity in presence H₂O and SO₂ [2,13]. Thus, the Pt-based catalysts show a great potential for the purification of CO in industrial flue gas.

Hence, in this work, the effects of H₂O, SO₂ and coexistence of H₂O and SO₂ on the catalytic oxidation of CO were researched over the 0.1Pt/TiO₂-A. Stability evaluation was also performed, which is essential for practical industrial applications. Attention has been particularly paid on the XPS results to reveal the changes in chemical properties by H₂O as well as SO₂ over the surface of the 0.1Pt/TiO₂-A. Combine with the results of TEM, XPS characterization, in situ DRIFTS measurements, H₂¹⁸O isotope-labeling experiments, the reaction mechanism of H₂O promoting CO oxidation on 0.1Pt/TiO₂-A catalyst was proposed.

2. Experimental

2.1. Catalyst preparation

The 0.1Pt/TiO₂-A catalyst was prepared through the impregnation method. About 15 g anatase TiO₂ (99.8%; Aladdin) was dried in a blast furnace at 110 °C for 12 h to remove the adsorbed water. The support (10 g) was added to 80 mL of deionized water. The solution of H₂PtCl₆ (8 wt.%; Aladdin) was then added into the above suspension, and the mixture was stirred at 60 °C for 2 h. The solvent was removed using a rotary evaporator at 60 °C. The obtained solid was dried in a blast furnace at 110 °C overnight, and finally calcined in a muffle furnace at a ramp rate of 8 °C min⁻¹ from 25 °C to 500 °C and maintained at 500 °C for 2 h. The required catalysts with 0.1wt.% Pt loading was obtained (The actual content of Pt measured by ICP-OES was 0.098wt.%) and the catalyst was denoted as 0.1Pt/TiO₂-A.

In order to reveal the influence of the existence of H₂O and SO₂ on the catalyst, 0.1Pt/TiO₂-A samples were pretreated under the reaction condition of 1% CO, 16% O₂, 10% H₂O and 1% CO, 16% O₂, 10% H₂O, 50 ppm SO₂ at 230 °C for 12 h. The catalysts were marked as 0.1Pt/TiO₂-W-12 and 0.1Pt/TiO₂-WS-12, respectively. Additionally, the 0.1Pt/TiO₂-A samples were pretreated under the reaction condition of 1% CO, 16% O₂, 10% H₂O, 50 ppm SO₂ at 230 °C for 6 h and 24 h and compared with the treatment for 12 h to reveal the deposition of sulfate species on the catalyst surface, and the catalysts were marked as 0.1Pt/TiO₂-WS-6 and 0.1Pt/TiO₂-WS-24, respectively. Before the reaction, the samples were pretreated with 400 mL/min N₂ purged at 300 °C for 1 h. In addition, the sample was cooled to room temperature by 400 mL/min N₂ purged after the reaction.

2.2. Catalyst characterization

Powder X-ray diffraction patterns were collected by using a Rigaku X'pert Pro diffractometer with Cu K α radiation (40 kV and 150 mA) at a scanning rate of 5 °/min over the 2θ range of 10–90°. Transmission electron microscopy (TEM) images and High-resolution transmission electron microscopy (HR-TEM) images of the samples were obtained on a JEM-2100 F microscopy operated at 200 kV. Energy-dispersive spectrometer (EDS) elemental mapping images of the samples were obtained using a high angle annular dark field (HAADF) detector under the scanning TEM mode on a high-resolution transmission electron microscope of OXFORD-80T. The chemical states and surface chemical composition of the samples were explored by X-ray photoelectron spectroscopy (XPS) measurements with Al K α (1486.8 eV) radiation source operated at 15 kV (ESCALAB 250Xi, Thermo Fisher, USA). The C 1s peak at 284.8 eV was used as an internal standard to calibrate the binding energy. The thermogravimetric data of the samples after reaction were obtained from 25 °C to 800 °C at a ramp rate of 5 °C/min by using DTG-60H (Shimadzu, Japan). All experiments were conducted at a N₂ flow rate of 50 mL/min. The actual Pt content of catalyst was analyzed by an inductively coupled plasma-optical emission spectrometer (ICP-OES, Optima5300DV, PerkinElmer). The Autosorb iQ system was used to measure the specific surface area of the samples by N₂ adsorption at -196 °C. Brunauer–Emmett–Teller (BET) equation was used to calculate specific surface area (S_{BET}) of samples from N₂ adsorption isotherm. The total pore volume (V_{pore}) was determined by the N₂ adsorption capacity at p/p₀ = 0.99. The pore distribution (D_{pore}) was calculated by the Barrett–Joyner–Halenda (BJH) method using the isotherm data.

2.3. Catalytic evaluation

The CO oxidation activities were performed in a continuous flow fixed-bed quartz microreactor (i.d. = 8 mm) with the prepared catalyst (400 mg, 40–80 mesh). In all activity tests, the total flow rate of the feed gas was 400 mL/min, with a gas hourly space velocity (GHSV) of approximately 60000 mL g⁻¹ h⁻¹. The reaction conditions were as follows: 1% CO, 16% O₂, 1–20% H₂O (when used), 5–500 ppm SO₂ (when used) and N₂ as the balance gas. High purity water was injected through a syringe pump into the quartz tube (300 °C) in the first furnace to vaporize to produce H₂O, which was carried by 100 mL/min N₂ and mixed with the reaction gas before entering the reaction tube. Moreover, the insulated inlet pipeline was maintained above 80 °C to avoid condensation of H₂O. The CO concentrations in the inlet and outlet were continuously analyzed using Fourier transform infrared (FTIR) spectroscopy (Tensor 27, Bruker, Germany). The conversion of CO is calculated by Eq. (1):

$$X = \frac{(N_{CO,inlet} - N_{CO,outlet})}{N_{CO,inlet}} * 100\% \quad (1)$$

Where X is the CO conversion, and N_{CO,inlet} and N_{CO,outlet} are inlet and outlet concentration of CO (ppm).

2.4. In situ DRIFTS experiments

In situ DRIFTS were recorded by MCT detector (using liquid nitrogen cooling) a stainless steel in-situ cell (Harrick) fitted with ZnSe window and a heating cartridge. Before the experiments, the in-situ cell was purged with N₂ at 400 °C (100 mL/min for 2 h). Subsequently, the powder sample (0.1Pt/TiO₂-A or SiC (99.9%; Macklin)) about 50 mg was placed on the supported disk and heat treated with 100 mL/min N₂ at 300 °C for 2 h. For the CO chemical adsorption experiment, the sample was cooled to 100 °C and the background spectrum was collected. Next, CO gas (1% CO, 100 mL/min) was fed for 0.5 h at 100 °C, and then N₂ gas was introduced to the sample for 0.5 h. For the CO

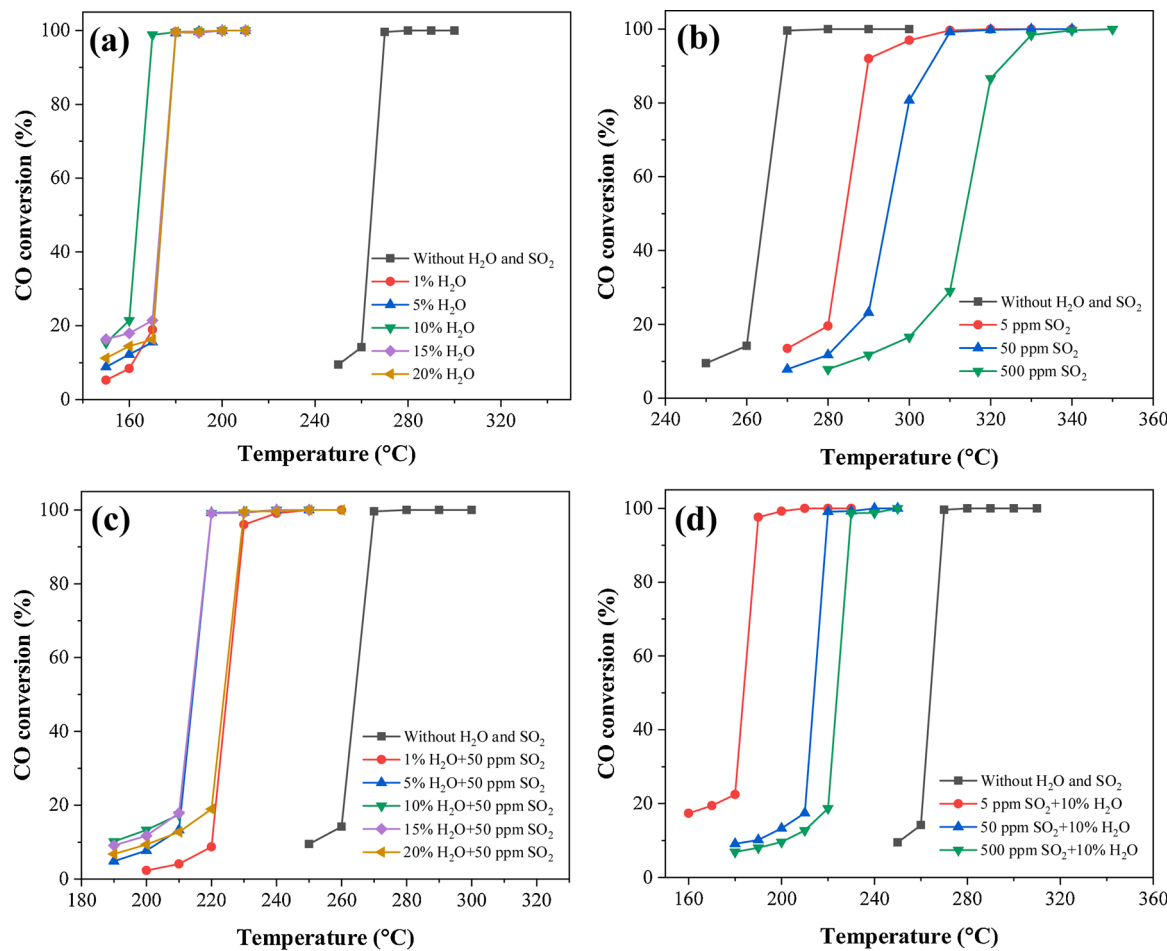


Fig. 1. Influence of single and complex atmosphere on CO catalytic oxidation activity over 0.1Pt/TiO₂-A catalysts. Reaction conditions: 1% CO, 16% O₂, 1-20% H₂O, 200 ppm NO (a) 1% CO, 16% O₂, 200 ppm NO, 5-500 ppm SO₂ (b) 1% CO, 16% O₂, 1-20% H₂O, 200 ppm NO, 50 ppm SO₂ (c) 1% CO, 16% O₂, 10% H₂O, 200 ppm NO, 5-500 ppm SO₂ (d), N₂ as balance gas, and GHSV: 60000 mL·g⁻¹·h⁻¹.

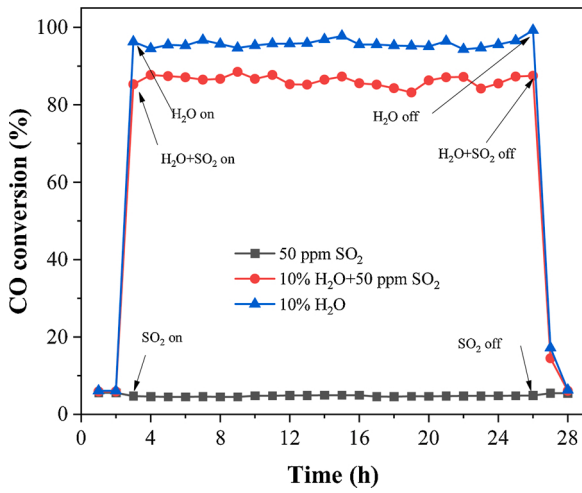


Fig. 2. Stability evaluation of 0.1Pt/TiO₂-A catalyst under different reaction atmosphere at 230 °C. Reaction conditions: 1% CO, 16% O₂, 200 ppm NO and other gases, GHSV: 120000 mL·g⁻¹·h⁻¹.

reaction experiment, the sample was cooled to 230 °C and the background spectrum was collected. Eventually, the IR spectra were collected at different times in a flowing stream (100 mL/min) including 1% CO, 16% O₂, and 1% CO, 16% O₂, 10% H₂O, N₂, respectively.

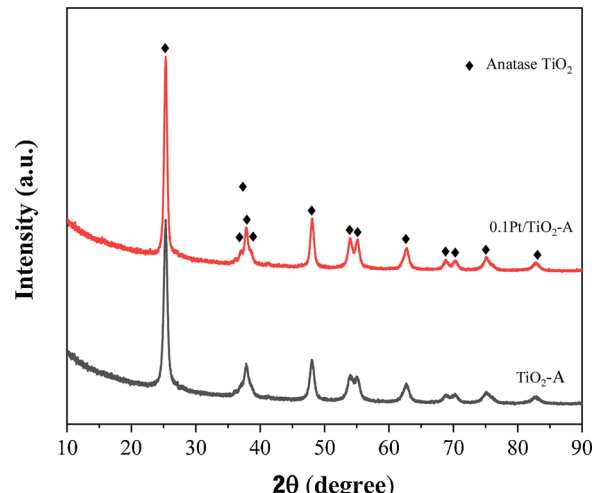


Fig. 3. XRD patterns of carrier TiO₂-A and 0.1Pt/TiO₂-A sample.

2.5. H₂¹⁸O isotope labeling experiments

For the H₂¹⁸O isotope labeling experiments, the gas at the outlet of fixed-bed tubular quartz was analyzed by online mass spectrometry (InProcess Instruments GAM-200). The catalyst was heated to 300 °C for 0.5 h under Ar atmosphere to purify before H₂¹⁶O and H₂¹⁸O engaging

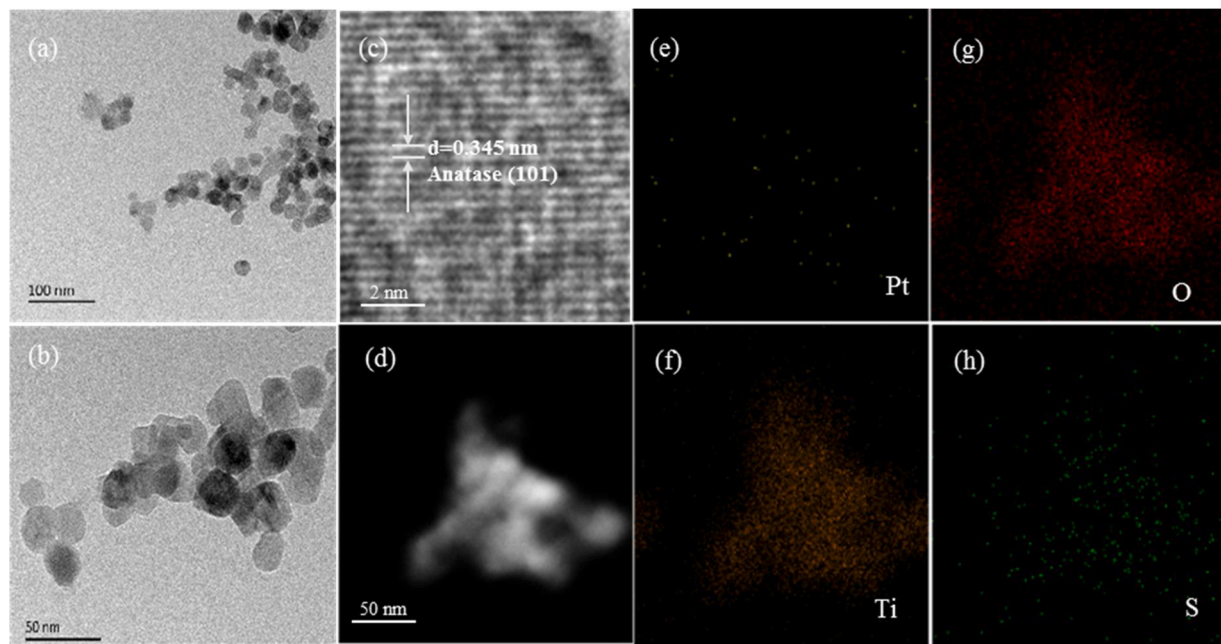


Fig. 4. TEM images (a, b) and HR-TEM images (c) of 0.1Pt/TiO₂-A sample; HADDF-STEM image (d) and STEM-EDS maps of 0.1Pt/TiO₂-A-WS-12 sample.

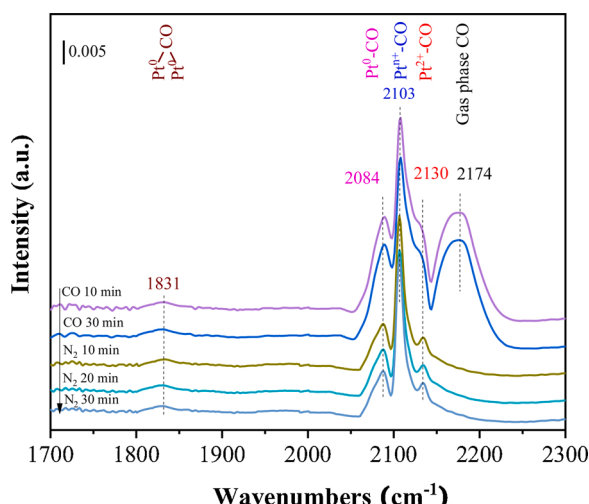


Fig. 5. In-situ DRIFT spectra of CO chemisorption on 0.1Pt/TiO₂-A catalyst at 100 °C.

experiments. 200 mL/min mixture of 1% CO, 16% O₂, 5% H₂¹⁶O, Ar as balance gas (a) or 1% CO, 16% O₂, 5% H₂¹⁸O (97%; Macleans), Ar balance gas (b) were purged into the catalytic system containing 200 mg of 0.1Pt/TiO₂-A (maintaining at 230 °C) at 1600 s and 11400 s with a GHSV=60000 mL·g⁻¹·h⁻¹, respectively. The C¹⁶O₂ mass spectrum signal values of the product after the reaction are marked as A and B, respectively. The proportion of C¹⁶O¹⁸O in the products of total CO₂ (C¹⁶O¹⁸O and C¹⁶O₂) can be calculated by the Eq. (2):

$$Y = \left(1 - \frac{B}{A} \right) * 100\% \quad (2)$$

3. Results and discussion

3.1. CO catalytic activity evaluation

The actual sintering flue gas inevitably emits H₂O and SO₂.

Therefore, it is meaningful to investigate the effect of H₂O and SO₂ on the CO catalytic oxidation of CO. As illustrated in Fig. 1a and b, compared with the dry conditions (T₁₀₀ = 270 °C), the introduction of H₂O into the reaction atmosphere significantly promoted the performance of CO catalytic oxidation. The promoting effect of H₂O on the catalytic oxidation of CO was consistent with the previously reported results [33,34]. Within the H₂O concentration range from 1% to 20%, 10% H₂O contributed the highest catalytic activity (T₁₀₀ = 170 °C). However, the introduction of SO₂ into the reaction atmosphere inhibited the catalytic oxidation of CO (Fig. 1b), the inhibition effect was stronger with the increase of SO₂ concentration.

Furthermore, the catalytic performance of 0.1Pt/TiO₂-A in presence of H₂O and SO₂ was also investigated. As illustrated in Fig. 1c and d, when SO₂ concentration (50 ppm) was fixed, introduction of 5%–15% H₂O contributed the lowest T₁₀₀ at 220 °C. In Fig. 1d, when H₂O concentration was set 10%, increase of the SO₂ concentration led to the decrease of the catalytic activity. Noteworthy, compared with the conditions without H₂O and SO₂, the promotion effect of H₂O was apparent even under harsh reaction conditions (10% H₂O, 500 ppm SO₂). Besides, the CO conversion suddenly jumped from less than 30%–100%, which was attributed to the rapid increase of the catalyst surface temperature owing to the release of a large amount of chemical heat after ignition of CO oxidation [43].

3.2. Stability evaluation

The catalytic stability is a very important factor of the catalyst, which is crucial to the industrial applications. Therefore, the catalytic stability of 0.1Pt/TiO₂-A in CO oxidation was evaluated at 230 °C. As shown in Fig. 2, the CO conversion was almost 5.9% in the first 2 h (CO + O₂ + NO). However, when 10% H₂O was introduced (CO + O₂ + NO + H₂O), the CO conversion rapidly increased (less than 20 min) to 96.3 % and maintained around 96% in the following 24 h. After H₂O was cut off, the CO conversion decreased to 17.2%. More importantly, when H₂O and SO₂ were introduced into the reaction atmosphere at the same time (CO + O₂ + NO + H₂O + SO₂), it could be observed that the CO conversion is slightly lower than only introducing H₂O. But it can still maintain around 85% for 24 h, confirming the high stability of 0.1Pt/TiO₂-A. When only SO₂ was introduced into the reaction atmosphere (CO + O₂ + NO + SO₂), the CO conversion is about 5%. These results were consistent

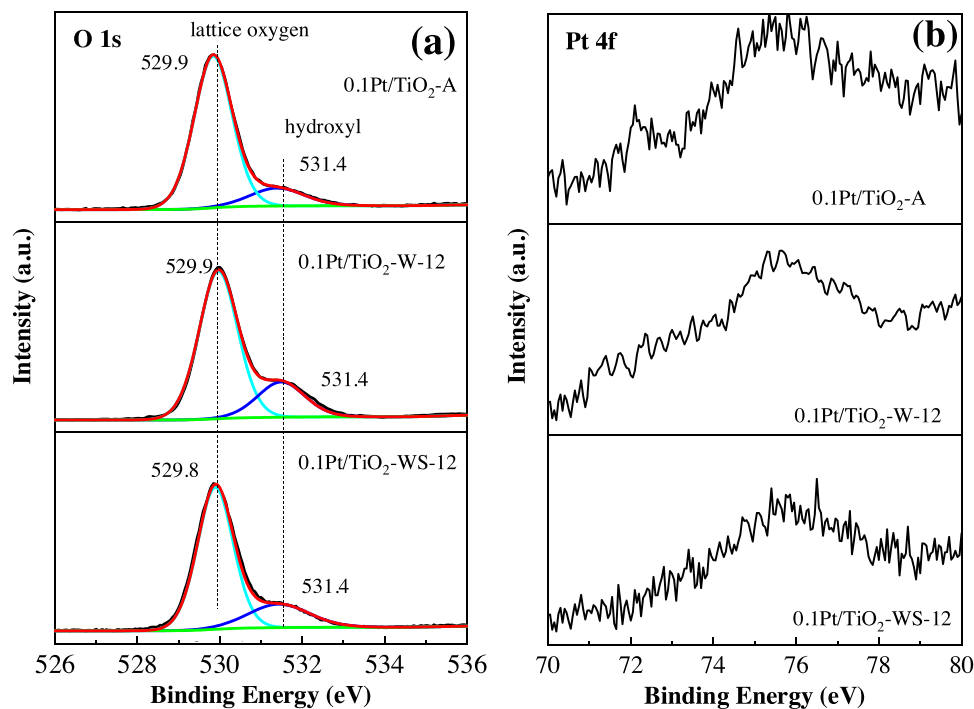


Fig. 6. O 1s and Pt 4f XPS spectra of 0.1Pt/TiO₂-A, 0.1Pt/TiO₂-W-12 and 0.1Pt/TiO₂-WS-12 samples.

Table 1
The O_{hydr}/(O_{hydr}+O_{latc}) ratio of the samples.

Sample	Binding Energy (eV)		O _{hydr} /(O _{hydr} +O _{latc})
	O _{latc}	O _{hydr}	
0.1Pt/TiO ₂ -A	529.8	531.4	0.145
0.1Pt/TiO ₂ -W-12	529.9	531.4	0.231
0.1Pt/TiO ₂ -WS-12	529.9	531.4	0.225

with previous research showing that H₂O could considerably promote the CO catalytic activity [12,33,44,45]. Accordingly, it can reasonably propose that H₂O alter the pathway of the CO catalytic oxidation reaction on the 0.1Pt/TiO₂-A catalysts. Furthermore, it can be seen that the promotion effect of H₂O was significantly greater than the inhibition effect of SO₂.

3.3. Catalyst characterizations

XRD patterns of support anatase-TiO₂, 0.1Pt/TiO₂-A sample were shown in Fig. 3. The peaks ($\theta = 25.35, 37.00, 37.88, 38.65, 48.14, 54.00, 55.15, 62.77, 68.88, 70.39, 75.17, 82.88^\circ$; PDF 21-1272) were attributed to anatase-TiO₂ and no characteristic peaks of Pt particles appear. This result indicated that Pt is uniformly dispersed on the surface of the anatase TiO₂ support.

Fig. 4a and b showed TEM images of the synthesized 0.1Pt/TiO₂-A sample. It could be seen that there was no obvious Pt nanoparticle, indicating that Pt has a very high degree of dispersion on the 0.1Pt/TiO₂-A sample. This could be caused by the extremely low Pt loading, which was consistent with the XRD results. HR-TEM image (Fig. 4c) clearly showed the lattice spacing of the anatase. In order to further analyze the distribution of Pt and S species on the catalyst surface, HAADF-STEM and STEM-EDS maps of 0.1Pt/TiO₂-WS-12 sample were collected. As illustrated in Fig. 4d-h, the catalyst was observed as high-density metals in the dark field scanning mode. In the STEM-EDS mapping (Fig. 4e-h), O (red) and Ti (orange) S (green) are clearly displayed. Pt species was hardly observed only as dispersed bright spot due to its very low loadings. Besides, S deposition clearly appeared on the used catalyst surface,

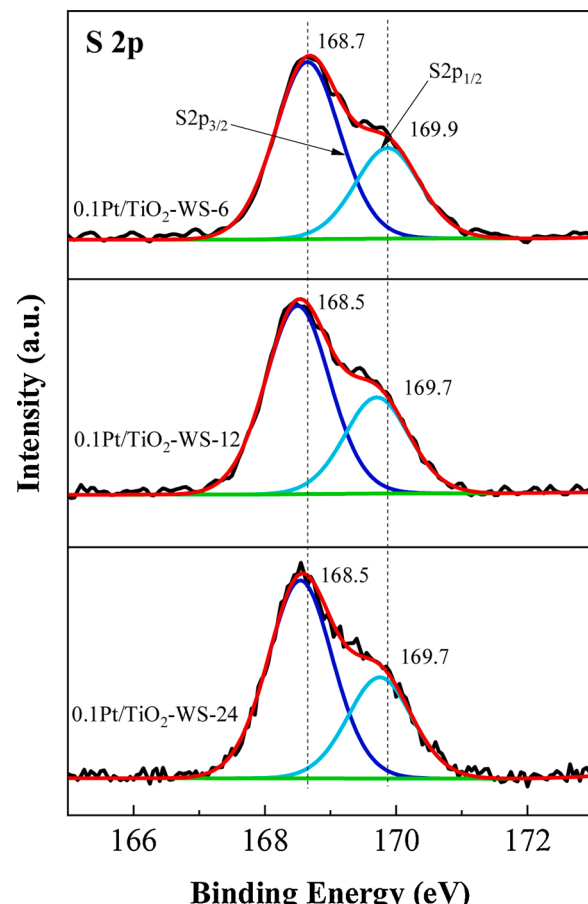


Fig. 7. S 2p XPS spectra of the 0.1Pt/TiO₂-WS-6, 0.1Pt/TiO₂-WS-12 and 0.1Pt/TiO₂-WS-24 samples.

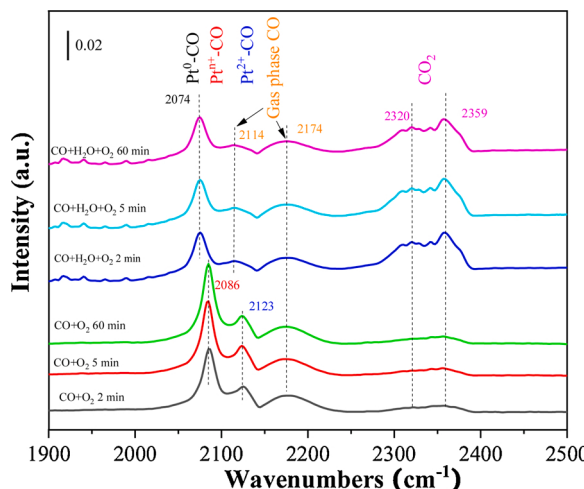


Fig. 8. In-situ DRIFT spectra of CO oxidation over 0.1Pt/TiO₂-A catalyst without H₂O or with 10% H₂O at 230 °C.

0.1Pt/TiO₂-A, the hydroxyl groups over the catalysts surface were significantly increased after treatment under the reaction conditions with only H₂O, and the highest value (0.231) of O_{hydr}/(O_{hydr}+O_{lattc}) ratio was obtained. In addition, the O_{hydr}/(O_{hydr}+O_{lattc}) ratio of the sample treated with H₂O and SO₂ coexisting was 0.225, which was slightly lower than that of single H₂O treatment. The remarkable increasing of hydroxyl groups on the catalyst surface was due to the dissociation of H₂O [33]. Fig. 6b showed the Pt 4f XPS spectra of fresh and used samples, and the corresponding peaks appeared at 72–78 eV, which was in accordance with previous literatures [49].

Besides, XPS characterization was also conducted over the samples treated with H₂O and SO₂ coexisting with different times. As shown in Fig. 7, the peaks with binding energy at around 168.7 eV and 169.9 eV were attributed to S 2p_{3/2} and S 2p_{1/2} of sulfate species, respectively [42]. In addition, our BET test results (Fig. S1 and Table S1) shown that the average pore diameter of the 0.1Pt/TiO₂-A catalyst (fresh and used) is about 14 nm. It reported that sulfuric acid is not easy to accumulate in the pores of 0.1Pt/TiO₂ samples with an average pore diameter greater than 10 nm [2]. Therefore, the sulfate species characterized by XPS should be mainly attributed to TiOSO₄ species [13]. Hence, the decrease

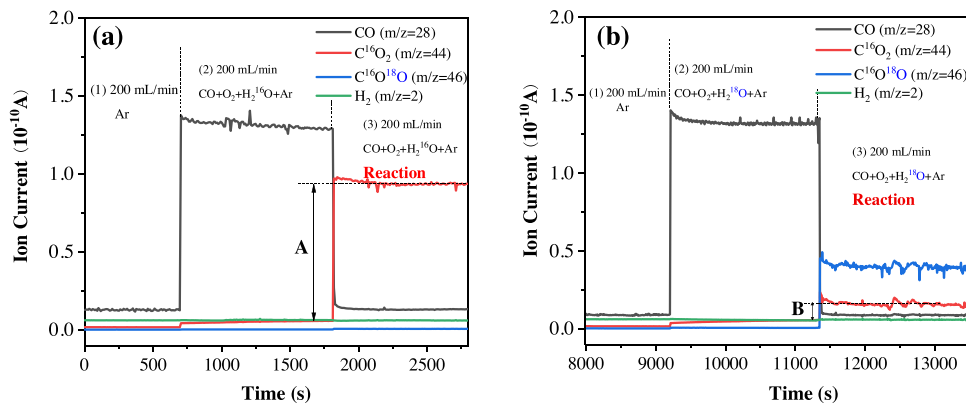


Fig. 9. Isotope-labeling experiments under 1% CO, 16% O₂, 5% H₂¹⁶O (a) or 5% H₂¹⁸O (b) conditions at 230 °C.

which was consistent with the following XPS results.

In-situ DRIFT spectra using CO as the probe molecule is an excellent method to prove the dispersed state of Pt. Here, the in-situ DRIF spectra CO chemisorption measurements were conducted on the 0.1Pt/TiO₂-A sample at 100 °C. As shown in Fig. 5, the infrared peak at 2174 cm⁻¹ was assigned to gaseous CO. The infrared peaks appearing at 2130 cm⁻¹ and 2103 cm⁻¹ were assigned to linearly CO adsorbed on Pt²⁺ and Ptⁿ⁺ ($1 < n < 2$) sites, respectively. The infrared peaks at 2084 cm⁻¹ and 1831 cm⁻¹ were attributed to linear coordinated and bridging CO on Pt⁰ sites [46–48], respectively. Although the Pt loading on the 0.1Pt/TiO₂-A catalyst is very low (0.1%), there still exists Pt⁰ species proving by the in-situ infrared of CO chemisorption. Therefore, this evidences strongly certified that Pt is dispersed in the form of small nanoparticles on 0.1Pt/TiO₂-A catalyst [48].

In order to analyze the changes of species and chemical states over the catalyst surface after the reaction of H₂O and H₂O coexisting with SO₂, the samples were characterized by XPS. Fig. 6a showed the O 1s XPS spectra of samples, which could be divided into two peaks. The main peak appearing at low binding energy (around 529.9 eV) was attributed to the lattice oxygen on the catalyst surface (Noted as O_{lattc}). A broad peak with a low binding energy (around 531.4 eV) was attributed to the hydroxyl groups on the catalyst surface (Noted as O_{hydr}) [32,33]. The oxygen in hydroxyl groups (O_{hydr}) on the catalyst surface plays a significant role in the catalytic oxidation of CO [49,50]. The ratio of O_{hydr}/(O_{lattc}+O_{hydr}) was calculated based on the corresponding peak area and the result was listed in Table 1. Compared with the

Table 2

The proportion of C¹⁶O¹⁸O in the products of total CO₂ at 230 °C and 260 °C.

Temperature/°C	Y/%
230	88.9
260	88.3

in CO catalytic activity is attributed to the formation of TiOSO₄ on the surface of 0.1Pt/TiO₂-A sample. More importantly, the proportion of surface S atoms of 0.1Pt/TiO₂-WS-6, 0.1Pt/TiO₂-WS-12 and 0.1Pt/TiO₂-WS-24 samples were 3.10%, 3.02% and 3.29%, respectively. It showed that the amount of S deposited on the catalyst surface did not increase with extension of time, which might be an important reason for the high sulfur resistance of 0.1Pt/TiO₂-A.

The amount of the sulfate species on used samples was also estimated from the thermogravimetric (TG) studies (Fig. S2). Based on previous reports, the temperature below 400 °C is commonly attributed to the weight loss of H₂O, and 400 °C–800 °C is ascribed to the thermal weight loss caused by sulfate decomposition over Pt/TiO₂ catalyst [2,13]. Therefore, the weight loss percentages above 400 °C of 0.1Pt/TiO₂-WS-6, 0.1Pt/TiO₂-WS-12 and 0.1Pt/TiO₂-WS-24 samples were 2.34%, 2.28% and 2.32%, respectively, which was consistent with XPS results.

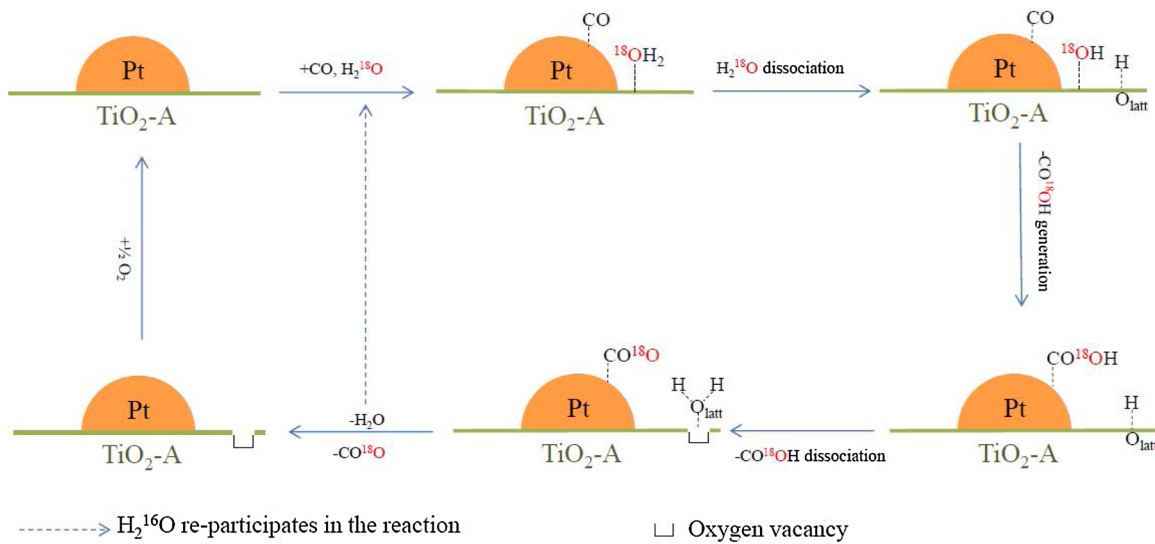


Fig. 10. Proposed water-promoting CO catalytic oxidation reaction mechanism at the Pt-TiO₂ interface.

3.4. In situ DRIFTS measurements

In order to further analyze the mechanism of H₂O promoting the catalytic oxidation of CO over 0.1Pt/TiO₂-A, in-situ DRIFTS experiments were conducted at 230 °C with 1% CO, 16% O₂, 10% H₂O (when used), N₂ (Fig. 8). Additionally, Collecting a reference spectrum on inert materials under the same reaction condition could correct the interference of gas phase CO peaks on adsorbed CO peaks at Pt sites during DRIFTS analysis [51]. In this work, the DRIFT spectra of SiC samples which has not CO adsorption peaks (Fig. S3) were recorded (Figs. S4–S5). Based on the result of Figs. 8 and S3–S5, the infrared peak appearing at 2300–2400 cm⁻¹ was attributed to gas phase CO₂. The infrared peak appearing at 2174 cm⁻¹ and 2114 cm⁻¹ were assigned to gas phase CO. The infrared peaks at 2123 cm⁻¹ and 2074 cm⁻¹ were attributed to the linear CO species adsorbed on Pt²⁺ and Pt°, respectively. The infrared peak at 2086 cm⁻¹ was to CO adsorption on Ptⁿ⁺ (1 < n < 2) [10,49]. When 10% H₂O was introduced, the gas phase CO₂ peak increased significantly indicating that H₂O apparently promoted the catalytic oxidation of CO, which was consistent with the conclusion of the activity evaluation. After the introduction of H₂O, the absorption peaks intensity of CO decreased demonstrating that high concentration of H₂O (10%) competed with CO for adsorption on Pt sites. Moreover, the peak of Pt°–CO species appeared indicating that the Pt species in oxidation state on the catalyst might have been reduced [33]. CO adsorption on Pt° species was easier to desorb than CO adsorption on Ptⁿ⁺ species [52]. Therefore, this could be one of the reasons for H₂O promoting the catalytic oxidation of CO.

3.5. H₂¹⁸O isotope-labeling experiments

In order to further investigate the effect of H₂O on the mechanism of CO catalytic oxidation, H₂¹⁸O isotope-labeling experiments were conducted over 0.1Pt/TiO₂-A, and the reaction products were analyzed by Mass spectrometry. When H₂¹⁶O was added to the reaction atmosphere (Fig. 9a), the reaction products showed a negligible amount of C¹⁶O¹⁸O (*m/z* = 46) and a main signal of C¹⁶O₂ (*m/z* = 44) at 230 °C. When H₂¹⁸O was added to the reaction atmosphere (Fig. 9b), the reaction products showed a relatively lower signal of C¹⁶O₂ (*m/z* = 44) and a higher signal of C¹⁶O¹⁸O (*m/z* = 46) at 230 °C, and the amount of C¹⁶O₂ in the reaction product was reduced by 88.9%, indicating that the proportion of C¹⁶O¹⁸O in the total CO₂ was 88.9%. Furthermore, the result of 260 °C showed great consistency as 230 °C (Table 2). When only H₂¹⁸O and C¹⁶O₂ was cuted into the catalyst maintaining at 230 °C, the signal value

of C¹⁶O¹⁸O has not changed significantly, indicating that the *OH groups on the surface of the catalyst has negligible effect on the ¹⁸O isotope labeling experiment (Fig. S6).

When CO and H₂O are present in the reaction atmosphere over Pt-based catalysts, the product of CO₂ may be caused by Water Gas Shift (WGS) reaction (CO+H₂O→CO₂+H₂). Hence, the signal value of H₂ (*m/z* = 2) was detected. It was found that the signal value of H₂ (*m/z* = 2) was not increased in whole reaction process, indicating that CO₂ was not generated by WGS reaction. Besides, the remaining about 11% of C¹⁶O₂ (*m/z* = 44) may be caused by impure heavy oxygen water (97% H₂¹⁸O), the generated H₂¹⁶O during the reaction re-participated in the catalytic cycle [34], and other CO oxidation pathways [53]. H₂¹⁸O isotope-labeling experiments unambiguously confirmed that the direct involvement of H₂O in the catalytic oxidation of CO over 0.1Pt/TiO₂-A, responsible explicitly for 88.9% the amount of the final CO₂ formation.

3.6. Water-promoting CO catalytic oxidation mechanism

In recent years, the results obtained by Density Functional Theory (DFT) or kinetic calculations in many publications [32,33,44,54] showed that the fast reaction between *CO and *OH at the metal-support interface generated the key intermediate product *COOH species (carboxyl), which is extremely easy dehydrogenation to form CO₂. The *OH originated from the continuous dissociation of H₂O on the surface of the support, which was consistent with our results measured by XPS (Fig. 6a). For example, Zhao et al. [44] studied by the operando DRIFTS investigation confirmed that H₂O continuously replenished the consumed *OH groups during the reaction process. The DFT calculation results show that the *COOH species generated by *CO and *OH at the interface is easily decomposed (0.09 eV), which is a key step for H₂O to promote catalytic oxidation of CO (Eq 3). Furthermore, our H₂¹⁸O isotope-labeling experiments unambiguously proof that the presence of H₂O in the reaction atmosphere changed the reaction pathway of CO catalytic oxidation, resulting 88.9 % of C¹⁶O¹⁸O production at 230 °C. Combining our experimental results and previous calculation models [33,34,44,45], when H₂O entered in the reaction atmosphere, the CO catalytic oxidation reaction pathway over the 0.1Pt/TiO₂-A catalyst was reasonably proposed (Fig. 10).



Consequently, the reaction steps were: CO adsorption on Pt sites; H₂¹⁸O dissociation to hydroxyl groups (-¹⁸OH) on metal oxide surface; reaction between adsorbed CO and hydroxyl (-¹⁸OH) to form -CO¹⁸OH

species; $-CO^{18}OH$ species decomposition into $CO^{18}O$ and $-H$, Meanwhile, $-H$ combining with lattice hydroxyl ($-OH$) to generate $H_2^{16}O$; Gas phase O_2 supplement oxygen vacancies to complete the catalytic cycle.

4. Conclusions

In this work, H_2O significantly enhance the catalytic oxidation of CO over 0.1Pt/TiO₂-A. SO_2 can inhibit the catalytic oxidation of CO. When H_2O and SO_2 coexist in the reaction atmosphere, the promoting effect of H_2O is greater than the inhibiting effect of SO_2 . More importantly, 0.1Pt/TiO₂-A also exhibited superior endurance for coexisting H_2O and SO_2 at 230 °C. The introduction of H_2O into the reaction atmosphere would cause the Pt species in the oxidation state to be reduced to Pt^0 , which weakened the adsorption strength of CO. The dissociation of H_2O over the catalyst surface led to remarkably increase of hydroxyl groups, which could be the key oxides to react with adsorbed CO at metal-support interface. The $H_2^{18}O$ isotope-labeling experiments unambiguously proof that the presence of H_2O in the reaction atmosphere changed the reaction pathway of CO catalytic oxidation, resulting 88.9% of $C^{16}O^{18}O$ production. Accordingly, water-promoting CO catalytic oxidation reaction mechanism at the Pt-TiO₂ interface was proposed.

CRediT authorship contribution statement

Chenglin Feng: Writing - original draft, Visualization, Data curation, Conceptualization. **Xiaolong Liu:** Conceptualization, Writing - review & editing, Supervision, Project administration, Funding acquisition. **Tingyu Zhu:** Writing - review & editing, Supervision, Project administration, Funding acquisition. **Yutao Hu:** Visualization, Data curation. **Mengkui Tian:** Visualization.

Declaration of Competing Interest

The authors report no declarations of interest.

Acknowledgements

This work was supported by National Key Research & Development (R&D) Program of China (No. 2018YFC0213400; 2017YFC0210500) and the National Natural Science Foundation of China (51938014).

Appendix A. Supplementary data

Supplementary material related to this article can be found, in the online version, at doi:<https://doi.org/10.1016/j.apcata.2021.118218>.

References

- [1] B. Ozturk, O. Arihan, F. Coskun, N.H. Dikmenoglu-Falkmarken, Clin. Hemorheol. Micro 61 (2016) 591–597.
- [2] K. Taira, K. Nakao, K. Suzuki, H. Einaga, Environ. Sci. Technol. 50 (2016) 9773–9780.
- [3] T. Fujita, T. Ishida, K. Shibamoto, T. Honma, H. Ohashi, T. Murayama, M. Haruta, ACS Catal. 9 (2019) 8364–8372.
- [4] V.V. Dutov, G.V. Mamontov, V.I. Zaikovskii, O.V. Vodyankina, Catal. Today 278 (2016) 150–156.
- [5] Z. Li, H. Wang, W. Zhao, X. Xu, Q. Jin, J. Qi, R. Yu, D. Wang, Catal. Commun. 129 (2019), 105729.
- [6] A. Tomita, K.-i. Shimizu, K. Kato, T. Akita, Y. Tai, J. Phys. Chem. C 117 (2013) 1268–1277.
- [7] M. Piumetti, T. Andana, S. Bensaid, D. Fino, N. Russo, R. Pirone, AIChE J. 63 (2017) 216–225.
- [8] D. Mukherjee, B.G. Rao, B.M. Reddy, Appl. Catal. B: Environ. 197 (2016) 105–115.
- [9] Y.-X. Miao, J. Wang, W.-C. Li, Chin. J. Catal. 37 (2016) 1721–1728.
- [10] H. Liu, L. Ma, S. Shao, Z. Li, A. Wang, Y. Huang, T. Zhang, Chin. J. Catal. 28 (2007) 1077–1082.
- [11] K. Liu, A. Wang, T. Zhang, ACS Catal. 2 (2012) 1165–1178.
- [12] J. Lin, B. Qiao, L. Li, H. Guan, C. Ruan, A. Wang, W. Zhang, X. Wang, T. Zhang, J. Catal. 319 (2014) 142–149.
- [13] K. Taira, H. Einaga, Catal. Lett. 149 (2019) 965–973.
- [14] N. Kamiuchi, M. Haneda, M. Ozawa, Catal. Today 201 (2013) 79–84.
- [15] H. Liu, A. Jia, M. Yuwang, J. Luo, Lu, Chin. J. Catal. 36 (2015) 1976–1986.
- [16] C.-H. Jung, J. Yun, K. Qadir, B. Naik, J.-Y. Yun, J.Y. Park, Appl. Catal. B Environ. 154–155 (2014) 171–176.
- [17] M. Shen, G. Wei, H. Yang, J. Wang, X. Wang, Fuel 103 (2013) 869–875.
- [18] C.W. Chao Wang, Jochen Lauterbach, Erdem Sasmaz, Appl. Catal. B Environ. 206 (2017) 1–8.
- [19] S. Wei, X.-P. Fu, W.-W. Wang, Z. Jin, Q.-S. Song, C.-J. Jia, J. Phys. Chem. C 122 (2018) 4928–4936.
- [20] G. Peng, L.R. Merte, J. Knudsen, R.T. Vang, E.L. Gsgaard, F. Besenbacher, M. Mavrikakis, J. Phys. Chem. C 114 (2010) 21579–21584.
- [21] E. Kolobova, A. Pestryakov, G. Mamontov, Y. Kotolevich, N. Bogdanchikova, M. Farias, A. Vosmerikova, L. Vosmerikova, V. Cortes Corberan, Fuel 188 (2017) 121–131.
- [22] X. Zhang, S. Cheng, W. Zhang, C. Zhang, N.E. Drewett, X. Wang, D. Wang, S.J. Yoo, J.-G. Kim, W. Zheng, Ind. Eng. Chem. Res. 56 (2017) 11042–11048.
- [23] L.-L. Zhang, M.-J. Sun, C.-G. Liu, Mol. Catal. 462 (2019) 37–45.
- [24] J. Lin, Y. Huang, L. Li, A. Wang, W. Zhang, X. Wang, T. Zhang, Catal. Today 180 (2012) 155–160.
- [25] W.C. Li, H.H. Zhang, J.T. Wang, W.M. Qiao, L.C. Ling, D.H. Long, Adv. Mater. Interfaces 3 (2016), 1500711.
- [26] S. Mo, Q. Zhang, Y. Sun, M. Zhang, J. Li, Q. Ren, M. Fu, J. Wu, L. Chen, D. Ye, J. Mater. Chem. A 7 (2019) 16197–16210.
- [27] L.R.M. Guowen Peng, Jan Knudsen, Ronnie T. Vang, Erik Lægsgaard, Flemming Besenbacher, Manos Mavrikakis, J. Phys. Chem. C 114 (2010) 21579–21584.
- [28] E. Moretti, L. Storaro, A. Talon, P. Patrono, F. Pinzari, T. Montanari, G. Ramis, M. Lenarda, Appl. Catal. A Gen. 344 (2008) 165–174.
- [29] Y. Yang, H. Dong, Y. Wang, C. He, Y. Wang, X. Zhang, J. Solid State Chem. 258 (2018) 582–587.
- [30] Y. Zhou, Z. Wang, C. Liu, Catal. Sci. Technol. 5 (2015) 69–81.
- [31] P. Landon, J. Ferguson, B.E. Solsona, T. Garcia, S. Al-Sayari, A.F. Carley, A. A. Herzing, C.J. Kiely, M. Makkee, J.A. Moulijn, A. Overweg, S.E. Golunski, G. J. Hutchings, J. Mater. Chem. 16 (2006) 199–208.
- [32] T. Wang, J.-Y. Xing, A.-P. Jia, C. Tang, Y.-J. Wang, M.-F. Luo, J.-Q. Lu, J. Catal. 382 (2020) 192–203.
- [33] T. Wang, J.-Y. Xing, L. Zhu, A.-P. Jia, Y.-J. Wang, J.-Q. Lu, M.-F. Luo, Appl. Catal. B Environ. 245 (2019) 314–324.
- [34] C. Wang, X.-K. Gu, H. Yan, Y. Lin, J. Li, D. Liu, W.-X. Li, J. Lu, ACS Catal. 7 (2016) 887–891.
- [35] M. Date, M. Okumura, S. Tsubota, M. Haruta, Angew. Chem. Int. Ed. 43 (2004) 2129–2132.
- [36] J. Saavedra, C.J. Pursell, B.D. Chandler, J. Am. Chem. Soc. 140 (2018) 3712–3723.
- [37] M.L. Kazemi, R. Sui, P.D. Clark, R.A. Marriott, Appl. Catal. A Gen. 587 (2019) 117–256.
- [38] P.D. Clark, R. Sui, N.I. Dowling, M. Huang, J.M.H. Lo, Catal. Today 207 (2013) 212–219.
- [39] M.R. Kim, S.I. Woo, Appl. Catal. A Gen. 299 (2006) 52–57.
- [40] D.L. Mowery, R.L. McCormick, Appl. Catal. B Environ. 34 (2001) 287–297.
- [41] M.B. Haebin Shin, Youngsoo Ro, Changyeol Song, Kwan-Young Lee, Kyu Song, Appl. Surf. Sci. 429 (2018) 102–107.
- [42] M.Y. Smirnov, A.V. Kalinkin, A.V. Pashis, I.P. Prosvirin, V.I. Bukhtiyarov, J. Phys. Chem. C 118 (2014) 22120–22135.
- [43] C.H. Jung, J. Yun, K. Qadir, B. Naik, J.Y. Yun, J.Y. Parka, Appl. Catal. B Environ. 154–155 (2014) 171–176.
- [44] S. Zhao, F. Chen, S. Duan, B. Shao, T. Li, H. Tang, Q. Lin, J. Zhang, L. Li, J. Huang, N. Bion, W. Liu, H. Sun, A.Q. Wang, M. Haruta, B. Qiao, J. Li, J. Liu, T. Zhang, Nat. Commun. 10 (3824) (2019).
- [45] S.C. Ammal, A. Heyden, ACS Catal. 4 (2014) 3654–3662.
- [46] Z. Jiang, Y. Yang, W.F. Shangguan, Z. Jiang, J. Phys. Chem. C 116 (2012) 19396–19404.
- [47] F.C. Meunier, L. Cardenas, H. Kaper, B. Smid, M. Vorokhta, R. Grosjean, D. Aubert, K. Dembele, T. Lunkenbein, Angew. Chem. Int. Ed. 60 (2021) 3799–3805.
- [48] Y. Zhou, D.E. Doronkin, M.L. Chen, S.Q. Wei, J.D. Grunwaldt, ACS Catal. 6 (2016) 7799–7809.
- [49] J. Liu, T. Ding, H. Zhang, G. Li, J. Cai, D. Zhao, Y. Tian, H. Xian, X. Bai, X. Li, Catal. Sci. Technol. 8 (2018) 4934–4944.
- [50] X. Zhao, Y. Hu, H. Jiang, J. Yu, R. Jiang, C. Li, Nanoscale 10 (2018) 13384–13392.
- [51] A. Paredes-Nunez, I. Jbir, D. Bianchi, F.C. Meunier, Appl. Catal. A Gen. 495 (2015) 17–22.
- [52] G.J. Kim, D.W. Kwon, S.C. Hong, J. Phys. Chem. C 120 (2016) 17996–18004.
- [53] D. Widmann, R.J. Behm, Acc. Chem. Res. 47 (2014) 740–749.
- [54] H.-F. Wang, R. Kavanagh, Y.-L. Guo, Y. Guo, G.-Z. Lu, P. Hu, Angew. Chem. Int. Ed. 51 (2012) 6657–6661.